Analysis of Lamellar Structure in Semicrystalline Polymers by Studying the Absorption of Water and Ethylene Glycol in Nylons Using Small-Angle Neutron Scattering

N. S. Murthy* and M. K. Akkapeddi

Engineered Materials Sector Research Laboratories, AlliedSignal Inc., Morristown, New Jersey 07962

W. J. Orts

USDA-ARS, Western Regional Research Center, CPU-800 Buchanan Street, Albany, California 94710

Received May 29, 1997; Revised Manuscript Received October 4, 1997[⊗]

ABSTRACT: Preferential diffusion of deuterated solvents into the amorphous regions of a semicrystalline polymer enhances the contrast between the crystalline and amorphous regions measurable by small-angle neutron scattering. This scattering in nylons from the diffusion of D_2O and deuterated ethylene glycol (d-EG) is analyzed by identifying the distinct contribution to scattering from the two amorphous regions, one in the interlamellar spaces and the other outside the lamellar stacks. The central diffuse scattering (I_d) is the non-Bragg, liquidlike, or independent scattering, and is attributed to the solvents (D_2O/d-EG) in the amorphous domains outside the lamellar stacks. The lamellar scattering (I_l) is the interference peak from the lamellae in the stacks and is used to evaluate the distance between the lamellae, the thickness of the interlamellar spaces, and the coherence length of the lamellar stacks. The invariant calculations show that 70%−80% of the lamellar stack is crystalline. About one-third of the amorphous material in a highly crystalline nylon is in the interlamellar space, and two-thirds is outside the lamellar stacks. The thickness of the interlamellar amorphous regions into which solvent molecules diffuse varies from 10 to 60 Å depending on the thermal history and is a major contributor to the observed increase in lamellae spacing. Structural changes in nylon 6 immersed in water are accelerated at 125 °C, and this temperature could be the hydrated-equivalent of the Brill transition observed at 160 °C in dry nylon 6. Water or EG diffuses into the fold surfaces of nylon lamellae at elevated temperatures, and subsequent structural changes are accompanied by hydrolysis of the nylon chains. EG being a stronger solvent reduces the lamellar thickness at elevated temperatures.

Introduction

The amorphous or the noncrystalline component constitutes 20% to 80% of a typical semicrystalline polymer and significantly affects the polymer properties such as processibility, dimensional stability, tenacity, fracture toughness, diffusion behavior, and aging characteristics. For instance, because the crystalline regions are essentially impermeable to solvents or gases, the diffusion behavior in semicrystalline polymers is determined by the density, orientation, and connectivity of the amorphous regions. Similarly, the amorphous domains, being the more mobile segment in a semicrystalline polymer, determine the deformation behavior of the polymer under impact. However, the analysis of the spatial distribution of the amorphous chain segments is not straightforward. Here we explore the possibility of characterizing the structure in noncrystalline regions, i.e., the local fluctuations in the average density and orientation of the amorphous chain segments,[1,2] by analyzing the distribution of gases and liquids in a polymer. The premise is that the amorphous regions that are less dense are likely to be more accessible to solvents (e.g., water for nylons) than those which are more dense.

Although some earlier reports[3,4] suggested that water penetrates into the crystalline domains in nylons, recent studies have show that diffusion occurs primarily through the amorphous regions of the polymer.[5−10] The Bragg-like peak in the small-angle neutron scattering (SANS) scans from nylons arises from the periodic fluctuations in the distribution of D_2O imposed by the lamellar structure.[6,8,10] The small changes in the arrangement of the crystalline stems within the lamellae that occur during hydration could be the result of specific interactions between water molecules and the noncrystalline segments in the interlamellar regions, possibly at the fold surface.[6] We also found that the H−D exchange of the protons on the amide group that accompanies the diffusion of water is reversible in the amorphous regions.[6] If the crystallinity is sufficiently low, i.e., if the chains are still relatively unconstrained and crystallizable, then this exchange can be accompanied by crystallization. Crystallization accompanied by H−D exchange transforms the amide group into ND in the presence of D_2O and into NH in the presence of H_2O. These can be reversed only under conditions more severe than that present during crystallization; i.e., if the crystallization takes place at 100 °C in the presence of D_2O, then some ND can be incorporated into the crystals by heating in the presence of H_2O at 120° C.

Our earlier work showed that water diffuses into two distinct amorphous domains—one in the interlamellar regions inside the lamellar stack and the other outside the lamellar stack.[6,10] Miura et al. report that NMR can distinguish constrained and free amorphous chain segments,[7] which we interpret as belonging to two different class of amorphous domains. Vergelati, Im-

* To whom correspondence should be addressed. Telephone: (973) 455-3764. Fax: (973) 455-5295. E-mail: nsmurthy@alliedsignal.com

[⊗] Abstract published in *Advance ACS Abstracts,* December 15, 1997.

S0024-9297(97)00760-2 CCC: $15.00
Published on Web 01/13/1998

berati, and Perez show that only a small amount (1%) goes into interlamellar amorphous phase, the remaining 8% being located in the intrinsic amorphous phase,[9] which could be what we refer to here as the amorphous phase outside the lamellar stack. Jin et al. postulated that water resides only in the activated (wholly amorphous) and not in the inactivated (intercrystalline) region to explain the large depression in the glass transition temperature (T_g) by small quantities of water.[11] Our own SANS work on fibers as well as solid-state NMR data supports this idea of two types of bound water,[12] in addition to a third, very mobile species most likely in the microvoids.[10,13] The two bound species can be associated with the two different amorphous domains. Sauer and Hsiao have shown that this feature is common to other semicrystalline polymers such as PET and PEEK.[14]

In this paper we further investigate the distribution solvents into the two amorphous regions, and their diffusion into the fold-surfaces of the lamellae by measuring the changes in the lamellar spacing and the thickness of the interlamellar spaces. These data enable us to evaluate the differences in the effect of water and ethylene glycol (EG) on the structure at the crystal−amorphous interface at elevated temperatures. We propose new methods for analyzing the small-angle scattering (SAS) data.

Experimental Methods

Nylon 6 (N6) film from AlliedSignal Inc. (Capron 77A) was used for most of the measurements. N6 plaques were injection molded from 8202NL (AlliedSignal) and nylon 6,6 (N66) plaques were molded from Zytel 101 (DuPont). The starting nylon 6 film (Film A) was not highly crystalline (∼15% crystallinity). A highly crystalline N6 film was prepared by annealing the film at 140 °C in H_2O (series H, H_2O-crystallized). The amide groups in the crystalline regions were labeled with deuterium (ND-c) by crystallizing the starting N6 in D_2O at 140 °C (series D, D_2O crystallized). This film was dried under dynamic vacuum at 50 °C and then exposed to H_2O at 70 °C to exchange the amorphous ND (ND-a) to NH (NH-a). An Anton-Paar high pressure bomb was used to anneal the samples at elevated temperature in water or other solvents.

In the notation used here, the amorphous and the crystalline regions are indicated by letters a and c, respectively. The dry samples will be identified by paired letters such as H−D; the first and the second letters of the pair refer to the nature of the amide group (H for protonated and D for deuterated) in the crystalline and the amorphous regions, respectively (the first letter is A for the starting film which is a mixture of H and D). For the hydrated samples, the second letter is replaced with D_2O or H_2O in as in H−D_2O for a nylon film with NH in the crystalline regions and D_2O in the amorphous regions.

The effect of temperature on the diffusion of water was studied by measuring the scattering at various temperatures from N6 immersed in D_2O. Measurements were also made after annealing the two nylons N6 and N66 for 2 h. at two nominal temperatures of 120 and 140 °C (actual temperatures could be up to ∼5 °C higher) in mixtures of water and deuterated-EG (d-EG of the type CD_2OHCD_2OH) with ratios of 100/0, 75/25, 50/50, 25/75, and 0/100.

All SANS measurements, including the high-temperature runs, were carried out with samples contained in an aluminum cell with quartz windows. SANS data from nylon films in D_2O were collected on the 30 m instrument at the National Institute of Standards and Technology. Most of the data were collected with a sample to detector distance of 2.5 m. The data were scaled to absolute values using a water standard. Radial scans were obtained from unoriented films by circular averaging. Data from nylon plaques in D_2O and H_2O/EG were collected at the Argonne National Laboratory's spallation source using the instrument SAD.

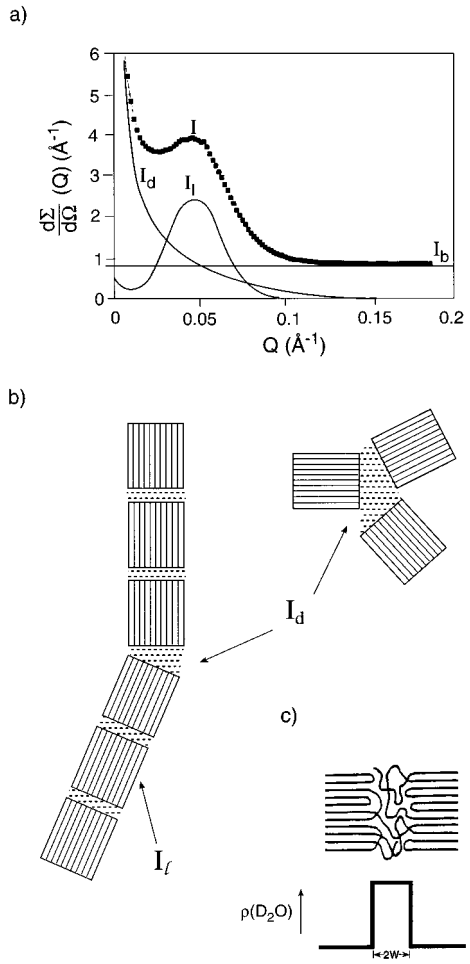

Figure 1. (a) Observed small-angle intensity (I) which is separated into I_b (background intensity. incoherent scattering in SANS), I_d (central diffuse scattering), and I_l (lamellar peak). (b) Schematic of the distribution of the amorphous chain segments and the crystalline stems in a semicrystalline nylon. (c) Model for the distribution of the D_2O.

Wide-angle X-ray diffraction (WAXD) data were obtained on a Philips diffractometer (PW 3710) in the parafocus geometry. The WAXD data were analyzed by profile fitting the scan between 10 and 35° in 2θ to amorphous and crystalline peaks to obtain a measure of the total crystallinity (crystalline index, CI) and crystallite size.[15] Crystallite size along the chain-axis was determined from the meridional (0, 14, 0) reflection from scans done on a Rigaku Dmax goniometer.

Differential scanning calorimetry (DSC) data from nylons in the presence of water and EG were obtained at a 10 °C/min heating rate in nitrogen on a TA instrument DSC2010 with samples sealed in stainless steel pans with rubber O-rings.

Data Analysis

SAS data from semicrystalline polymers have been analyzed both in real-space using correlation functions[16] and in the reciprocal space by fitting the data to the intensity calculated from a model.[17−19] We use the latter approach, but a different model. Our earlier studies,[6] as well as the data to be presented here, suggest that scattering of the type shown in Figure 1a could be separated into two components (Figure 1b): (1) the discrete scattering due to lamellae in the lamellar stacks in which the contrast is due to the regularly spaced interlamellar amorphous regions between the crystalline lamellae and (2) the diffuse scattering from the amorphous domains outside

the lamellar stacks or in isolated lamellae in which the contrast is between amorphous domains and the surrounding the crystalline regions. The two intensities are calculated as follows.

Consider the distribution of D_2O, or electron density for X-rays, to be a step function of width $2w$ (Figure 1c). The Fourier transform of this step function is[20]

$$F_{\text{step}}(w) = \sin(wq)/(wq) \tag{1}$$

where q ($= 4\pi(\sin\theta)/\lambda$) is the scattering vector in which 2θ is the scattering angle and λ is the wavelength.

The liquidlike, central diffuse scattering from independently scattering single step functions is given by[21]

$$J_{\text{d}}(q) = [AF_{\text{step}}(B)]^2 \tag{2}$$

where A is the intensity due to independent scatterers, and B is half the width of the step function. This diffuse scattering arises from regions containing nonlamellar crystallites, has a maximum at $q = 0$ Å^{-1}, and contributes to some of the background intensity under the lamellar peak.

The lamellar stack is the convolution of the lattice function with individual lamella. The scattering amplitude from these lamellar stack is the product of the Fourier transforms of the lamella and the lattice function. The lattice function is represented by a series of Gaussian peaks, two being sufficient in the angular range of our data. Thus, the intensity J_1 of the lamellar peak with a maximum at a q corresponding to the lamellar spacing is

$$J_1(\text{q}) = [F_{\text{step}}(C)\{\text{Gauss}(D,E,F) + \text{Gauss}(D,2E,F)\}]^2 \tag{3}$$

where

$$\text{Gauss}(D,E,F) = D\exp[-0.5((q-E)/F)^2] \tag{4}$$

C is half the thickness of the interlamellar amorphous layer between the lamellae in the lamellar stack, and D, E, and F are, respectively, the amplitude, position and width of the lattice function. The term $F(C)$ in eq 3 is the structure factor of the lamella, and Gauss(D,E,F) and Gauss(D,2E,F) are the first and the second order interference functions due to the lattice points. D represents the intensity due to the lamellar scattering. E and F are related to the lamellar spacing and the coherence length of the lamellar stack by eqs 5 and 6, respectively.

$$\text{lamellar spacing} = 2\pi/E \tag{5}$$

$$\text{coherence length} = 4\pi/[\sqrt{(8\ln 2)}F] \tag{6}$$

The observed intensity $I(q)$ is given by

$$I(q) = I_{\text{b}} + J_{\text{d}}(q) + J_1(q)/q^2 \tag{7}$$

I_{b} is the incoherent background. We attribute the diffuse scattering to the amorphous domains outside the lamellar stacks; they can be considered to be isotropic, and hence J_{d} is same as the observed central diffuse intensity $I_{\text{d}}(q)$. The lamellae are assumed to be disks and hence J_1 is divided by the Lorentz factor (q^2) to obtain the observed intensity $I_1(q)$. Parameters A–F were determined by least-squares fit of eq 7 to the observed data using the program PeakFit from Jandel.

The scattering length density b for amorphous and crystalline domains was calculated using the expression

$$b = \sum b_i X_i / \sum V_i X_i \tag{8}$$

in which

$$X_i = (w_i/\text{Mw}_i)/K \tag{9}$$

where b_i, V_i, w_i and Mw_i are, respectively, the scattering length, molar volume, the weight fraction and the molecular weight of the species i. K is a normalizing constant to make $\sum X_i$ equal to unity and can be set equal to 1. The species in our measurement are H_2O, D_2O, d-EG, and N–H and N–D nylons in the amorphous regions, and N–H and N–D nylons in the crystalline regions. The contrast contributing to the intensity is the difference between the scattering length densities of the crystalline (b_c) and the amorphous (b_a) regions. The invariant Q for the lamellae is given by

$$Q = \int_0^\infty I_1(q)\, q^2\, \text{d}q \tag{10}$$

and was calculated from the fitted parameters of the data by numerically integrating this expression from $q = 0.001$ to 10. A q_{max} of 10 was found to be reasonably close to ∞. The fitted parameters allow us to do this extrapolation to angles beyond the measured value. We found that the Q with a q_{max} of 0.25 (the upper limit of the data) was essentially same as that obtained with a q_{max} of 10. The relation between Q, contrast, volume fractions of crystalline (ϕ_{c}), and the amorphous ($\phi_{\text{a}} = 1 - \phi_{\text{c}}$) components is given by[22]

$$Q = 2\pi^2\phi_{\text{c}}\phi_{\text{a}}(b_{\text{c}} - b_{\text{a}})^2 \tag{11}$$

where b_{c} and b_{a} are the scattering lengths of crystalline and amorphous regions. The above expression was used to estimate the crystalline fraction within the lamellar stacks.

Results

The samples used in this study are listed in Table 1. The starting film (sample A) has low crystallinity (15%). When this film is immersed in D_2O, the crystallinity increases and the amide groups in both the newly formed crystallites and the amorphous regions become deuterated (see "Introduction"). More importantly, by annealing these films in D_2O or H_2O, the labeled amide groups are "locked" within the crystalline domains in the resulting highly crystalline (40% crystallinity) films. Thus, the amide groups in the crystalline regions are deuterated (ND-c) when annealed in D_2O (D series), or protonated (NH-c) when annealed in H_2O (H series). The contrast between the crystalline and amorphous regions depends on the composition in the crystalline and amorphous regions. Some of the scattering length densities are given in Table 2.

H_2O Crystallized Films (H). Both I_1 and I_{d} are intense in films exposed to D_2O (H–D_2O, Figure 2). These intensities almost disappear upon drying (H–D, Figure 3). Unlike the dried film H–H, the dried film H–D has a weak lamellar peak due to the H–D exchange in the amide groups on the amorphous chain segments (NH-a to ND-a), and for the same reason, a lower incoherent scattering. Figure 4 shows the temperature at which nylons (N66 plaques) are exposed to D_2O has a significant effect on the shape, position, and the intensity of the lamellar peak. The changes in I_{d} as well as in other features in the scans from N66 plaques annealed at 120 and 180 °C in D_2O are similar to those of the D_2O-crystallized films in H_2O (D–H_2O) and D_2O (D–D_2O), respectively.

D_2O Crystallized Films (D). Figure 2 shows that the central diffuse scattering I_{d} in films in which the amide groups in the crystalline region are ND and the film are kept moist with D_2O (D–D_2O) is the same as in a film in which the crystalline regions are "locked in" as NH and kept moist with D_2O (H–D_2O). A large decrease in the diffuse intensity I_{d} that occurs when the D_2O in the amorphous regions in the D films is

Table 1. Description of the Samples Used in This Study

sample identification[a]	sample treatment	nature of amide and water groups: crystalline region	nature of amide and water groups: amorphous region
A−D_2O	starting (low crystallinity) film in D_2O	ND, NH	ND, D_2O
	Films Crystallized (Annealed at 140°C) in H_2O		
H−H	Dried	NH	NH
H−D_2O	Dried/in D_2O	NH	ND, D_2O
H−D	Dried/in D_2O/ dried	NH	ND
	Films Crystallized (Annealed at 140°C) in D_2O		
D−D_2O	in D_2O	ND	ND, D_2O
D−D	dried	ND	ND
D−H_2O	dried and then in H_2O	ND	NH, H_2O
D−H	dried/in H_2O/dried	ND	NH
	Nylon Plaques		
N6	variable temperature data from RT to 150 °C in D_2O	NH,ND	ND, D_2O
N6	annealed at 120 °C and 140 °C in D_2O	NH,ND	ND, D_2O
N66	annealed at 120, 140, and 180 °C in D_2O	NH,ND	ND, D_2O
N6	annealed in water/d-EG mixture at 120 and 140 °C	NH	ND, d-EG
N66	annealed in water/d-EG mixture at 120 and 140 °C	NH	ND, d-EG

[a] The first letter of the pair such as H−D refers to the nature of the amide group in the crystalline regions, and the second to that in the amorphous regions; A is the starting film which has mixture of H and D in the crystalline regions. The second letter is replaced with D_2O or H_2O in hydrated samples as in H−D_2O.

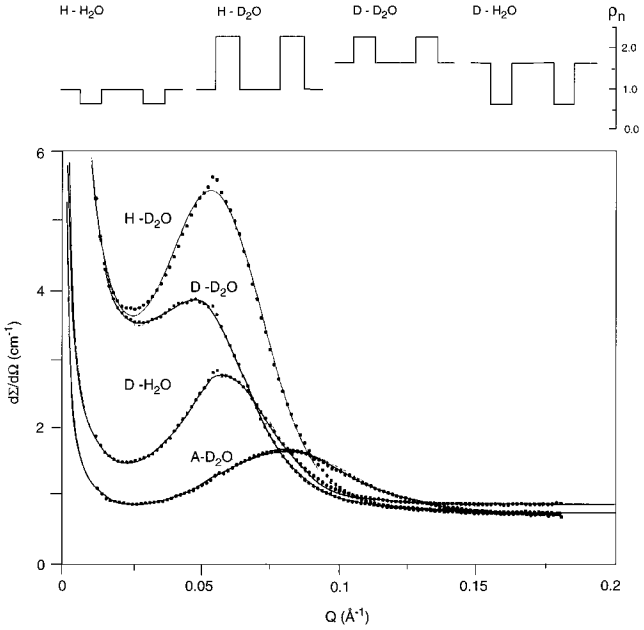

Figure 2. SANS data for films in D_2O. In this and the following figures, the points are the observed data and the smooth curve is the fit to the data according to eqs 1−7 on the basis of the model shown in Figure 1. The sample descriptions are given in Table 1. The scattering length contrast for which give rise to the intensity is also shown in the figure.

Table 2. Coherent Neutron Scattering Length Densities of Some of the Nylon Species

scattering entity	scattering length density(10^{-6} Å^{-2})
crystalline N6 (NH)	0.909
crystalline N6 (ND)	1.591
amorphous N6 (NH)	0.798
amorphous N6 (ND)	1.397
amorphous N6 (NH)−H_2O	0.589
amorphous N6 (ND)−D_2O	2.132
amorphous N6 (NH)−H_2O/d-EG	0.6 (100% H_2O) to 2.5 (100% d-EG)

exchanged with H_2O (D−D_2O to D−H_2O) is accompanied by only a small decrease in the lamellar intensity I_l. The lamellar peak in D−H_2O is weaker than in

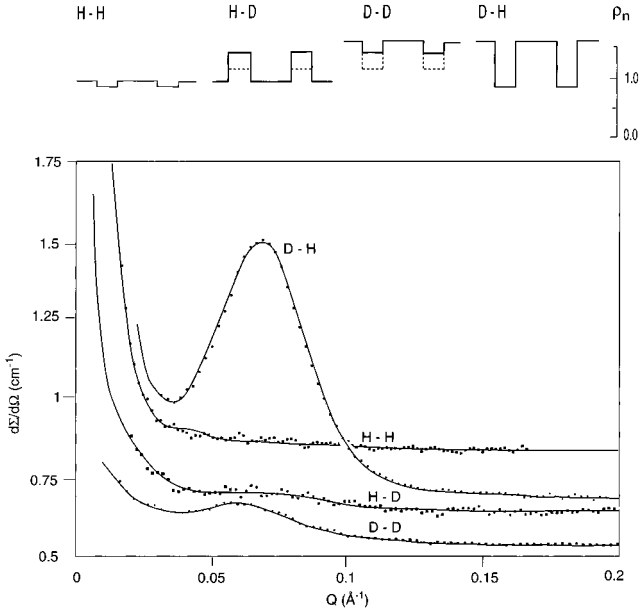

Figure 3. SANS data from dry films. The sample descriptions are given in Table 1, and the scattering length contrasts between the amorphous and the crystalline regions in the various samples are also shown in the figure.

H−D_2O, i.e., when the contrast is reversed, indicating that the scattering length density difference between the amorphous and the crystalline regions is smaller in ND-c and H_2O-a than in NH-c and D_2O-a (Figure 2). In addition to the differences in the intensities, the D_2O-crystallized films *appear* to have a larger lamellar spacing in D_2O than in H_2O, and this is completely reversible.

Variable-Temperature Measurements. Figure 5 shows some of the data obtained from N6 plaques immersed in D_2O at the temperatures indicated in the figure. The scans show that both the lamellar intensity and the lamellar spacing increase with temperature. These and other changes in the scans were analyzed by fitting the data to the six parameters as described 2under Data Analysis. The variations in the various parameters are plotted in Figure 6. The width of the amorphous domains outside the lamellar stacks (*B*) is

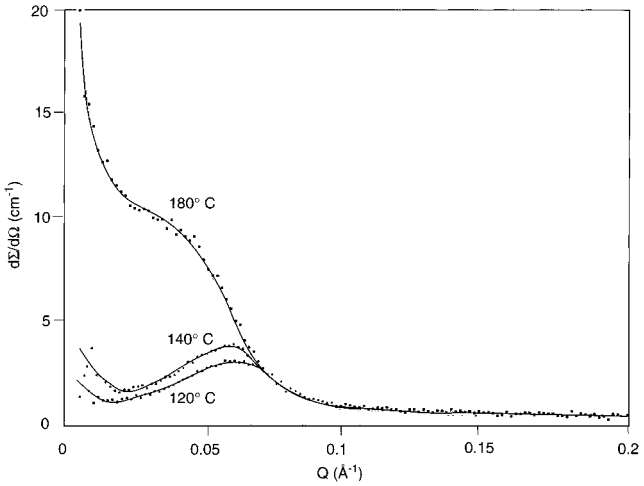

Figure 4. SANS data from N66 plaques treated with D_2O at three different temperatures.

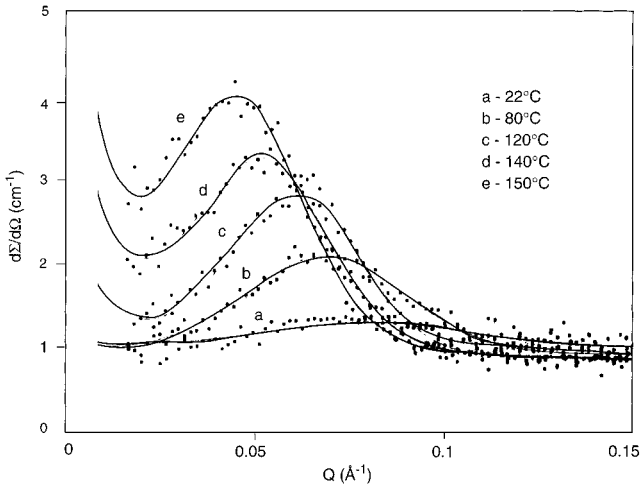

Figure 5. SANS data from nylon 6 in D_2O maintained at elevated temperatures during the measurement.

Table 3. Weight Gain (%) in Nylons in Water/Ethylene Glycol Mixtures

	nylon 6		nylon 66	
water/EG Ratio	120 °C	140 °C	120 °C	140 °C
100:0	9.3	9.3	6.9	7.9
75:25	13.5	15.4	9.8	11.7
50:50	17.1	24.7	16.0	15.5
25:75	23.4	28.4	19.3	20.7
0:100	30.5	39.3	22.4	22.9

not shown because the data do not extend to low enough q values, and therefore this particular parameter is not reliable. The data show the expected variations in these parameters and, interestingly, show accelerated change above 125 °C.

Diffusion of Water/ d-Ethylene Glycol. The data from N6 and N66 plaques exposed to water/d-EG under various conditions are shown in Figure 7 and the results are summarized in Figure 8. The results of weight uptake measurements in N6 and N66 plaques annealed at 120 and 140 °C in water/EG are summarized in Table 3. The SANS data at 25% EG are not given in Figure 8 because the SANS intensity is weak or absent at this EG concentration. The lamellar peak is clearly visible when nylons are exposed to H_2O, but disappears or is barely visible at 25% d-EG, and reappears as the ratio is increased to 50/50.

Table 4. Wide-Angle X-ray Diffraction Parameters in As-Molded and Water/Ethylene Glycol Treated Nylon Plaques[a]

			annealed			
			120 °D		140 °C	
nylon	structural parameter	as molded	H_2O	EG	H_2O	EG
N6						
	CI (%)	27	41	36	38	33
	α:γ	8:92	44:56	74:26	100:0	100:0
	CSP (Å): α1	68	104	124	142	139
	α2		57	68	74	67
	γ1	117	161	138		
	γ2	43	53	59		
	ICD $\Delta(2\theta)$ (deg)		3.844	4.026	4.046	4.055
	(0k0) CSP (Å)	35	46	46	50	46
N66	CI (%)	26	37	31	43	32
	CSP (Å): α1	76	72	77	88	95
	α2	49	47	51	50	51
	ICD $\Delta(2\theta)$ (deg)	2.871	3.242	3.500	3.573	3.489
	(0k0) CSP (Å)	37	40	40	46	52

[a] CI is the crystalline index, CSP is the crystallite size and perfection, α1, α2, γ1, and γ2 refer to lateral size, and (0k0) refers to the axial size; ICD is the index of crystalline density.

Wide-Angle X-ray Diffraction. WAXD scans of the N6 and N66 plaques annealed in water/EG are shown in Figure 9. The crystalline peak at $2\theta \sim 21°$ in some of these scans is due to the γ crystalline form (which occurs only in N6), and the peaks at $2\theta \sim 20°$ and 24° are due to the α crystalline form (which occurs in both N6 and N66). Annealing results in the transformation of γ to α in N6. The results are summarized in Table 4. The crystallinity is given in the form of a crystalline index (CI), which is the ratio of the area under the crystalline peaks to the total scattered intensity between the 2θ values of 10 and 35°. The crystallite sizes are listed as crystallite size and perfection (CSP) to emphasize that this size calculated from the Scherrer equation includes a contribution from defects, paracrystallinity and microstrain within the crystals. The CSP increases upon annealing at 120 °C in N6 and at 140 °C in N66. Another measure of the degree of perfection within the α crystals given in Table 4 is the index of crystal density which is the 2θ separation, $\Delta(2\theta)$, between its two intense reflections at ~20 and 24°. $\Delta(2\theta)$ increases mostly by the movement of the 24° peak to higher angles, and this corresponds to a decrease in the unit cell volume, i.e., an increase crystalline density.

Figure 10 shows examples of meridional scans through the (0, 14, 0) reflection used in the determination of the CSP's along the chain-axis. The data show that the apparent crystallite size is 35 Å in the as-molded plaques. The CSP increases by 5−15 Å upon annealing depending on the type of nylon, temperature, and the annealing medium (Table 4).

Discussion

We here analyze the SANS data for monitoring the distribution of solvents (water or EG for nylons) in the amorphous domains. Our representation of the distribution of D_2O as a step function is perhaps unrealistic. However, a model with a transition region between the amorphous and crystalline regions requires at least one additional parameter. Because our data can be fitted reasonably well to a step model, any additional parameter cannot be reliably determined from our data. Although we have previously attempted to determine the width of the diffuse boundary between the inter-

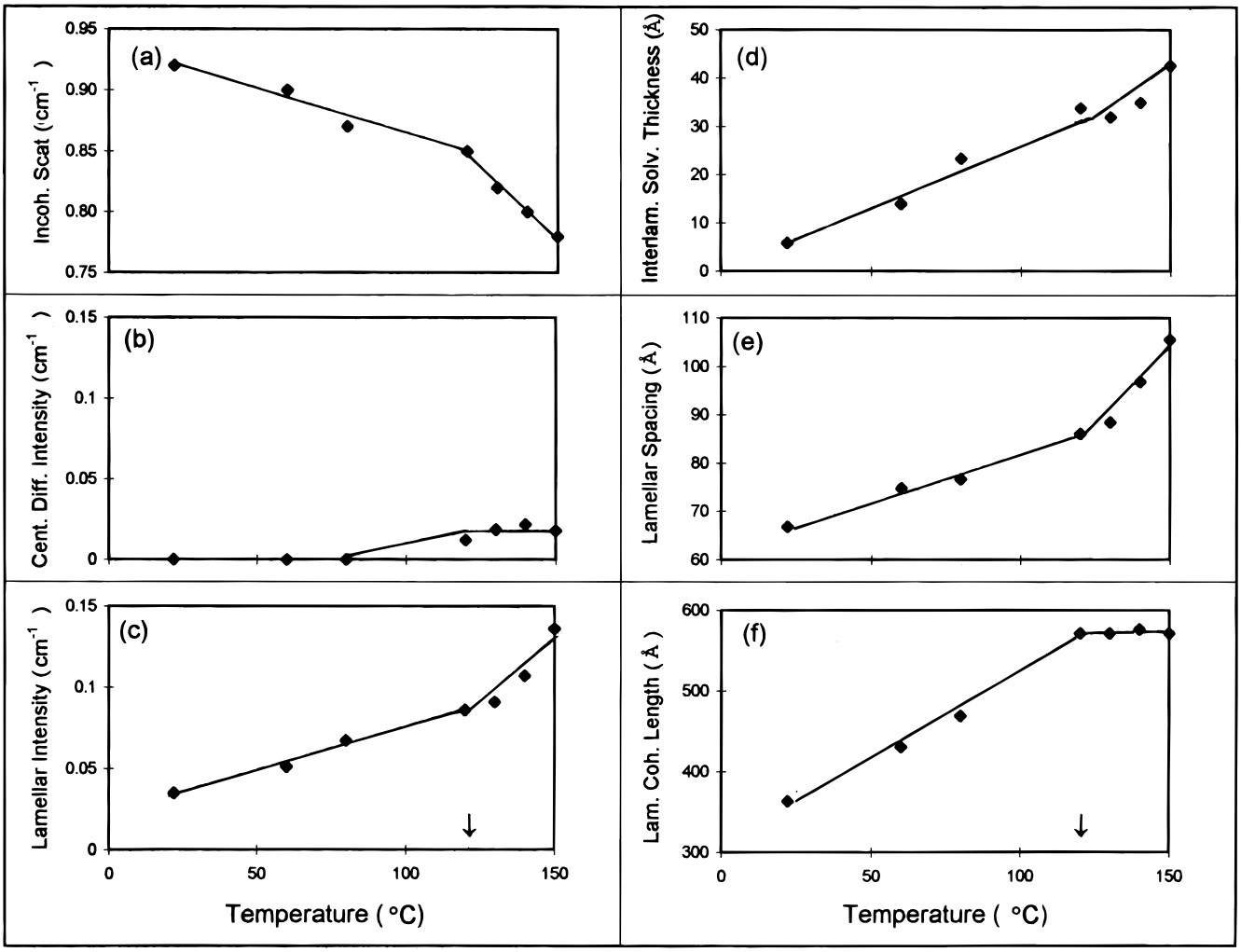

Figure 6. Summary of the fit of the variable-temperature SANS data. All the parameters except the width of the amorphous domains outside the lamellar stacks are plotted in the figure.

lamellar amorphous regions and the crystalline lamellae,[23] such analyses may not be meaningful because of the distribution in the lamellar spacings, the small size of domains, and because the samples are not ideal two-phase (amorphous and crystalline) systems. The commonly used correlation function analysis was not found useful because we have two scattering species, the independently scattering amorphous domains outside the lamellar stacks, which give rise to central diffuse scattering I_d, and the lamellar structures, which give rise to I_l.

We will interpret the data in terms of the six-parameter model (see Data Analysis) and use the model parameters to determine the following: (1) the number of incoherent scatterers from the base-line; (2) the fraction of independent scatterers from the central diffuse intensity A; (3) the size of the amorphous domains outside the lamellar stacks from B; (4) the thickness of the interlamellar amorphous domains from C; (5) the fraction of the lamellar scatterers from the lamellar intensity D; (6) the lamellar spacing from E; (7) the coherence length of the lamellar stack from F. The various parameters are plotted in Figure 6 for variable-temperature measurements, are summarized in Figure 8 for H_2O/d-EG samples, and are listed in Table 5 for all other samples.

Incoherent Scattering. The incoherent background scattering (I_b, base line at $q > 0.1$ Å^{-1}) is mostly proportional to the number of hydrogens (incoherent scattering lengths for ^{1}H and ^{2}H are 79.7 and 2.01 $\times$ 10^{-24} cm^2, respectively; it is zero for C, O, and N). Because the number of CH_2 units is the same in all the samples, I_b represents the number of NH and H_2O. I_b can be used as a measure of the amount of H_2O (Figure 11) as well as of the degree of exchange between ND and NH (see Effect of Temperature on Diffusion under Discussion). I_b reflects the crystallinity when the crystals are impermeable to the solvents. The I_b is highest in the H_2O-crystallized film (H−H), and decreases upon exposure to D_2O (H−D_2O) as a result of the conversion of NH-a to ND-a. The H−D and D−H films have the same incoherent scattering even though one is NH-c/ND-a and the other is ND-c/NH-a probably because both the films are roughly 50% crystalline. The film D−D has the least I_b because the only incoherent scatterers are the methylene hydrogens. The decrease in the incoherent scattering at higher temperatures in N6−D_2O (Figure 6) indicates increased H−D exchange.

Central Diffuse Scattering (I_d). Figures 2 and 4 show examples of the large changes in the monotonically decreasing diffuse scattering at $Q < 0.03$ Å^{-1}. I_d in small-angle literature on fibers is often attributed either to voids[5,24] or to fibrils.[10,25,26] I_d is typically known to increase upon annealing. It is possible that the topology of the connectivity between chain segments constrains the local volume to remain essentially unchanged during

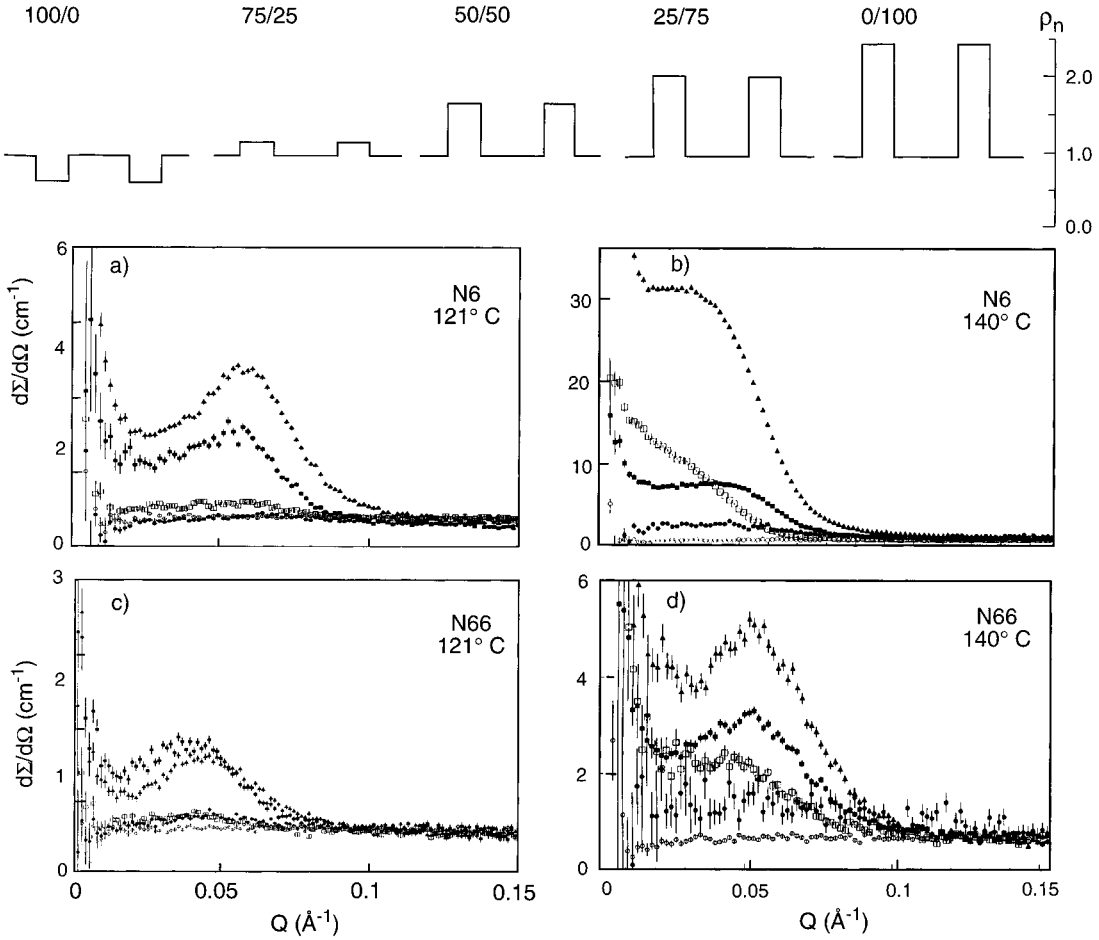

Figure 7. SANS data from N6 and N66 plaques annealed in water/EG mixture at 120 and 140 °C. Key: filled circle, 0/100 (H_2O); open circle, 25/75; open square, 50/50; filled square, 75/25; filled triangle, 0/100 (d-EG). Intensities have been divided by a hundred. The approximate (because EG varies with temperature and nylon type) scattering length contrasts for the samples at these five levels of EG are shown in the figure.

Table 5. Analysis of the Data Obtained at Ambient Temperature from Samples in D_2O Where the Six Parameters That Describe the Lamellar Structure and the Background Intensities Are Listed Below

		intensities (peak heights)			lamellar parameters (Å)			
sample ID	sample description	incoherent background	independent scatterers	lamellar stacks	lamellar spacing	coherence length	interlamellar amo−solvent domain width	size of the amo domains outside lam stacks (Å)
A−D_2O	as Rcd−D_2O	0.702	0.463	0.103	65	162	23	143
H−D_2O	NH−D_2O	0.698	1.991	0.178	89	205	42	156
H−D	NH−D_2O−dry	0.672	0.520	0.0547				164
D−D_2O	ND−D_2O	0.776	1.699	0.1444	88	184	49	176
D−D	ND−D_2O−dry	0.53	0.496	0.031	77	167	34	135
D−H_2O	ND−D_2O−dry−H_2O	0.868	1.021	0.11	88	227	35	156
D−H	ND−D_2O−dry−H_2O−dry	0.659	0.697	0.08	83	210	36	146
N6−D_2O	annealed at 120 °C	0.6	1.220	0.133	84	224	30	133
N6−D_2O	annealed at 140 °C	0.637	0.673	0.169	95	190	47	89
N66−D_2O	annealed at 120 °C	0.58	1.060	0.127	82	203	29	257
N66−D_2O	annealed at 140 °C	0.563	1.482	0.134	88	210	32	184
N66−D_2O	annealed at 180 °C	0.65	2.030	0.199	100	187	58	160

secondary crystallization, thus creating voids. These voids could be indistinguishable from the free volume, i.e., small enough not to cause any haze. Depending on the lower q-limit of the data, interfaces and density fluctuations also contribute to I_d. The size of the domain calculated from the width of I_d in our data is about 100−200 Å. Although the differences in this size in the various samples may not be meaningful (because data q_{min} is 0.005 $Å^{-1}$ and we assume a step-function), the changes in the intensity of the central diffuse scattering could be of some significance.

I_d is most intense when deuterated solvent (D_2O or d-EG) is present in the amorphous regions, decreases when D_2O is replaced with H_2O (e.g., D−D_2O to D−H_2O) even though the two scans show very similar lamellar peaks, and is the same in films H−D_2O and D−D_2O, which have different crystalline compositions (NH and ND) but about the same amount of D_2O in the amorphous regions. These results suggest that the I_d arises from the coherent, particulate-type scattering arising from the contrast generated by the D_2O-rich amorphous domains outside the lamellar stacks into which the

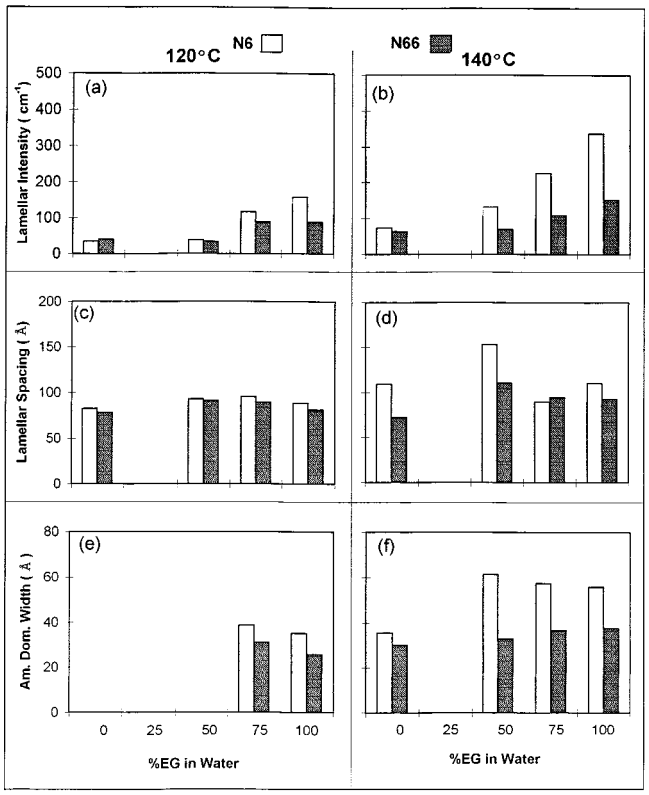

Figure 8. Summary of the effect of increase in the EG content in N6 and N66 at 120 and 140 °C.

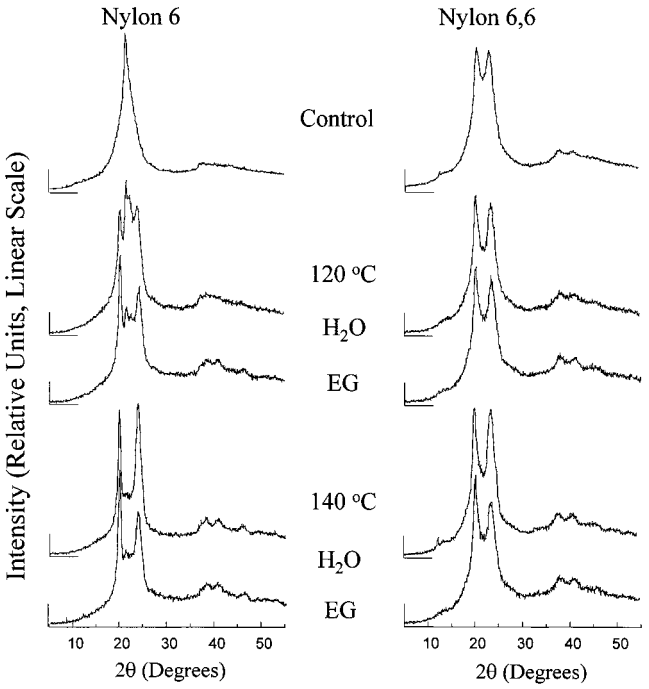

Figure 9. WAXD scans of the nylon 6 and nylon 6,6 plaques. As molded (control) plaques are at the top. Plaques annealed at 120 °C are in the middle. The plaques annealed at 140 °C are at the bottom.

solvent molecules also diffuse. If I_d in hydrated samples is due to the presence of D_2O in "voids", then I_d should be reasonably intense even when the films are dried. In contrast, we find that I_d decreases significantly upon drying (samples H−D and D−H in Figure 3) and is absent I_d in the dry film D−D. This suggests that there are contributions from species other than voids in the

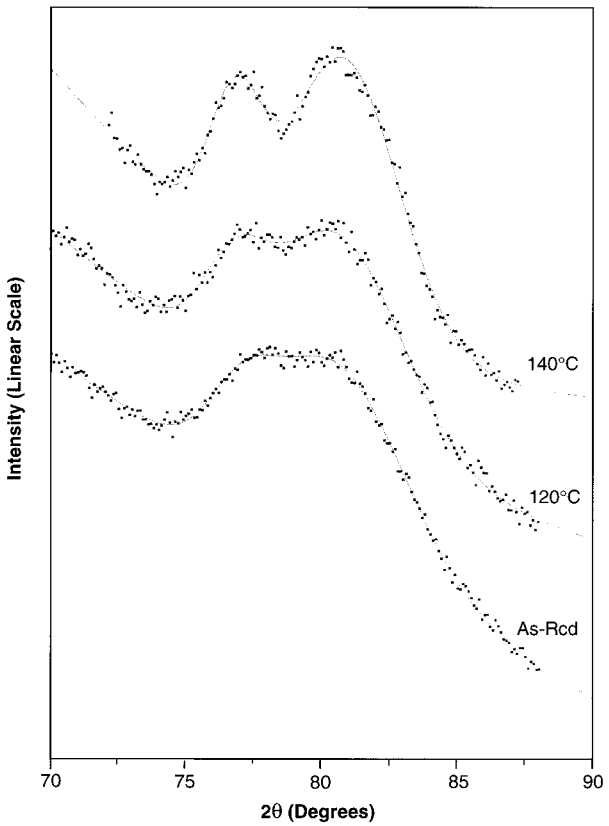

Figure 10. Wide-angle meridional scans from nylon 66 plaques before and after annealing.

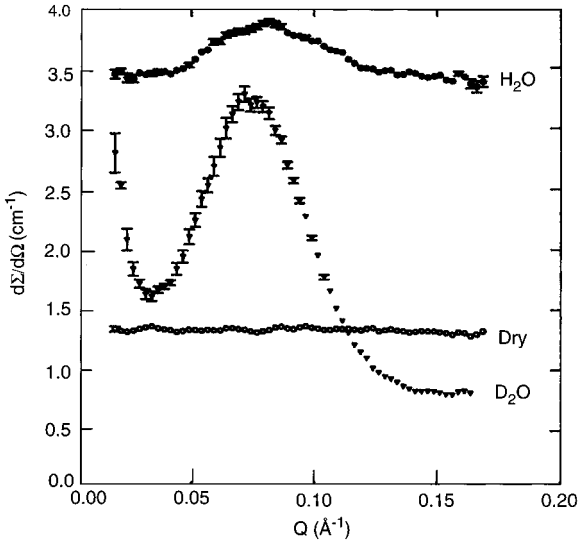

Figure 11. SANS data from nylon 6 fibers to illustrate the changes in the incoherent scattering due to different species in the amorphous regions.

q-range used here. An example could be D_2O in the amorphous regions between two lamellar stacks (Figure 1b).[27] I_d could also arise from the nonuniform distribution of solvents (D_2O/d-EG) outside the lamellar stacks because the amorphous regions are not uniformly accessible. Despite the larger amount of D_2O, the diffuse scattering I_d in A-D_2O is weaker than in H−D_2O, possibly because of the uniform distribution of D_2O outside the lamellar stack. For instance, in contrast to the annealed film, there could be fewer amorphous pockets between the lamellar stacks of the type shown in Figure 1b. Alternatively, a fewer number of lamellae

in the low crystallinity film A would reduce the contribution of the interfacial scattering to I_d.

Lamellar Peak (I_l). The contrast between the interlamellar amorphous regions and the lamellar crystals within the lamellar stacks gives rise to this lamellar interference peak. I_l in the starting film (A−D_2O) is weaker than in the H_2O-crystallized film (H−D_2O) despite the fact that the starting film, A, absorbs more D_2O (11% vs. 8%) because of its lower crystallinity in (Figure 1). Most of the D_2O in A-D_2O is in the amorphous regions outside the lamellar stack where they do not contribute to I_l. Although the starting film A crystallizes in the presence of D_2O and the amide groups in the crystalline regions become deuterated (ND-c), the contrast between ND-c and D_2O is large enough to give rise to an intense lamellar peak as seen in the scan from D_2O-crystallized film in D_2O (D−D_2O). The lamellar intensity I_l is somewhat weaker in the D−D_2O film than in the H−D_2O film, and this is to be expected from the scattering length density profile shown in Figure 2. In fact, the lamellar intensities observed in all our samples are consistent with the scattering length density profiles shown in this figure. The neutron scattering contrast in the dry, completely protonated nylon film H−H (NH-c, NH-a) is too small to give rise to a lamellar peak, but even if just the amide groups are deuterated, the resulting contrast is sufficient to give rise to the lamellar peak (Figure 3). Although lamellar intensity in the film D−H is the most intense as expected from the contrast, the observed intensity in the film D−D is more than that in H−D, opposite of what one would expect. It is possible that D to H exchange occurred in these two samples during drying, and this increases the contrast in D−D and decreases that in H−D (dotted lines in the contrast profile in Figure 3).

The invariant calculated from the data (eqs 10 and 11) showed that in all cases, irrespective of the crystallinity, the crystalline volume fraction within the lamellar stack is between 70% and 80%. Thus, only about one-tenth (in low crystallinity samples) to one-third (in high crystallinity samples) of the amorphous component in nylons is in the interlamellar regions within the lamellar stacks, and the remainder is outside the lamellar stacks. The large amorphous component outside the lamellar stacks and the density fluctuations within these domains contribute to the central diffuse scattering. The invariant for samples annealed in H_2O was between 4.1 and 4.9 compared to 2.6−3.2 (in units of 10^{-12} $Å^{-4}$) in films which were crystallized in the presence of D_2O. This suggests that by annealing the starting film in D_2O we have been able to convert only about half of NH in the crystalline regions to ND. These results are consistent with our previously published IR data.[6] Higher degrees of conversion are possible under more severe conditions

The lamellar spacing *appears to decrease* upon exchanging the D_2O in the interlamellar regions with H_2O (D- D_2O vs. D−H_2O, Figure 2). Although the lamellar spacings for the three samples D−D_2O, H−D_2O and D−H_2O calculated using eqs 1−7 are the same (88 Å), the peaks in the scans appear to shift progressively toward smaller *d*-spacings (0.0474, 0.0563, and 0.0587 $Å^{-1}$, corresponding to 133, 112, and 107 Å, respectively). These shifts are completely *reversible* as observed for instance in films with histories such as annealed in D_2O−dried−exposed to H_2O−dried−exposed to D_2O. The differences in the lamellar spacings between D−D_2O and D−H_2O is 25% before Lorentz factor correction (133 and 107 Å) and about half as much after the correction (105 and 93 Å). We attribute these differences to the difference in the structure factors of the scattering entities, i.e., the width of the step function, in the two samples, which modulates the intensity of the lamellar peak and contributes to the peak asymmetry by affecting the background underneath the lamellar peak. This is taken into account in our calculations by the width-factor *C*, in the shape function, $\sin(Cq)/(Cq)$ in eq 3, of the interlamellar amorphous regions. We find a systematic decrease in the thickness of the interlamellar solvent domains, 49, 42, and 35 Å, in D−D_2O, H−D_2O, and D−H_2O, respectively (Table 5). We suggest that these changes in the thickness results from the variations in the scattering length density profiles at the fold surface. The thickness is smaller in the unannealed film A despite the large amount of water in this sample, indicating that most of the D_2O in the unannealed samples is outside the lamellar stacks where it does not contribute to the lamellar scattering. At high temperatures, close to the hydrolysis temperature (∼150 °C in N6 and ∼180 °C in N66), the thickness of the D_2O-rich interlamellar amorphous domains in nylons approaches ∼60 Å.

In contrast to the above apparent shifts in the lamellar spacings, real increases in the lamellar spacing are often observed. For instance, when nylon is hydrated, the lamellar spacing increases reversibly from ∼80 Å in dry films to ∼ 90 Å. This increase is due to the swelling of the interlamellar regions, which contributes to the macroscopic increase in the volume of nylons exposed to moisture. The lamellar spacing are also known to increase upon annealing (e.g., compare A with other films in Table 5). Such increases could be due to an increase in the height of the lamellae, the interlamellar amorphous regions, or to a change in the distribution of lamellar spacings.

Effect of Temperature on Diffusion. Figure 6 shows the changes in the parameters used to fit the variable temperature SANS data. The background, which represents the incoherent scattering due to hydrogens on methylene and amide groups, decreases with temperature. Because the amide hydrogens can be exchanged with deuterium in D_2O, this continuous decrease in incoherent scattering suggests progressive H−D exchange. The <10 Å thick interlamellar regions at low temperatures does not represent a thin interlamellar amorphous layer but shows that water does not readily diffuse into the interlamellar amorphous domains at low temperatures. Both the lamellar spacing and the thickness of the interlamellar amorphous domains increase with temperature, but the difference between the two remains constant at about 60 Å over the entire temperature range. This value for the height of the lamellae is about the same as the crystal height after correction for microstrain broadening in highly crystalline N6 as measured by WAXD.[28] Thus, the increase in the lamellar spacing is probably due to an expansion of the interlamellar amorphous domains caused by the temperature and diffusion of water. Notice in these plots that the nature of the change in the structure accelerates at 125 °C: the incoherent background increases more rapidly; the central diffuse scattering appears; the lamellar intensity, the lamellar spacing, and the thickness of the interlamellar amor-

phous domain increases more rapidly; the coherence length of the lamellar stacks reaches a plateau. The rapid increase in the incoherent scattering indicates that the nylon crystals become permeable to water at 125 °C. These changes in the behavior could be due to onset of crystalline relaxation at this temperature analogous to that at the Brill transition temperature in dry nylons.[29,30] The Brill transition temperature in dry N6 is 160 °C, and the water would be expected to depress this temperature to 125 °C in the same way that it depresses the glass transition temperature in nylons. It is also known that to achieve a given structural state, the nylon 6 fibers need be annealed at a much lower temperature in the presence of moisture than that used for dry-annealing.[31] Thus, the SANS data in Figure 6 lead us to suggest the crystalline relaxation (usually called the α relaxation) which brings about the structural transformations at the Brill transition temperature also brings about changes in the organization of the lamellae.

Effect of Ethylene Glycol. We have so far discussed the diffusion of D_2O into nylons. We will now explore the usefulness of another probe, ethylene glycol. The purpose is 2-fold: first, the contrast can be varied by using mixtures of water and d-EG; second, we wanted to see how a solvent more efficient than water, such as EG, affects the nylons. The partially deuterated EG we used for SANS has only the hydrogen on the carbons deuterated while those on the hydrogen bonding hydroxyl group is unchanged (CD_2OHCD_2OH). This type of d-EG has the advantage over D_2O as a probe because the contrast is due only to the probe and not to ND resulting from the deuteron exchange. EG is fully miscible with water and is known to affect the properties of nylons more severely than water.

H_2O alone is sufficient to give rise to sufficient SANS contrast. The slight negative scattering length density at 100/0 H_2O/d-EG is compensated by d-EG at a 75/25 ratio (Figure 7). The contrast reappears at d-EG ≥50%, and the lamellar intensity increases with d-EG concentration due to the increase in the neutron scattering contrast. This increase is much larger in N6 than in N66 and is much larger at 140 °C than at 120 °C. The larger intensity in N6 relative to N66 is due to the higher amount of d-EG absorbed by N6. The variations in the SANS intensity in Figure 8 are in qualitative agreement with the contrast at various d-EG concentrations.

The data in Figure 8 show that the thickness of the interlamellar amorphous domains is larger in N6 than in N66 and is larger with EG than with H_2O. The thickness of the EG saturated interlamellar amorphous domains in N6 is 40 Å at 120 °C and increases to 60 Å at 140°C; the corresponding values in N66 are 30 and 40 Å. The lamellar spacing, after correcting for the Lorentz factor and shape factor, initially increases and then decreases with increase in EG, especially at 140 °C and in N6. The most plausible explanation is that at low EG concentrations, as EG diffuses into the interlamellar spaces, it swells the interlamellar amorphous phase and thus increases the lamellar spacing; at higher EG concentrations, EG begins to solvate the crystalline regions at the fold surface, and therefore decreases the lamellar spacings despite the increase in the thickness of the swollen interlamellar amorphous space. This decrease in the lamellar thickness in N6 at 140 °C in going from water to EG is confirmed by a decrease in the apparent crystal height (CSP, crystallite size and perfection from the meridional (0, 14, 0) reflection along the fiber-axis, Table 4) despite the increase in the crystalline perfection which would have increased the CSP. In contrast, the CSP in going from water to EG is unchanged at 120 °C in both in N6 and N66, and increases in N66 at 140 °C. These changes in height of the crystals are accompanied by changes in the lateral CSP (from ($h0l$) reflections) as well. The general increase in the lateral CSP upon annealing, because this is not accompanied by an increase in crystallinity, is due to an increase in crystalline perfection and not to an increase in the actual size. The decrease in lateral CSP in N6 at 140°C in EG is an exception to this, suggesting that the N6 crystals are indeed solvated under these conditions.

The crystal height L_{cr} obtained from the difference between L and L_{am}, is larger than the crystal height obtained from the width of the ($0k0$) reflections. L_{cr} is typically 40−50 Å (from Table 5) and is about 10 Å larger than the apparent crystallite size (CSP) from the ($0k0$) reflections (Table 4) because the latter has not been corrected for defects and microstrain which make the CSP lower than the actual crystal size. The decrease in crystallinity in going from water to EG, and the absence of a corresponding decrease in CSP (with the exception of N6 in EG at 140°C), suggests that EG mostly increases the crystal perfection (reduce the defects or distortions within the crystal lattice) rather than increase the actual height of the crystals. This could be brought about by the increased mobility at the water-swollen fold surface of the lamellae by either temperature or a solvent or, in this case, a combination of both. Note also that L_{cr} was essentially unchanged in the temperature range of our measurements in water but decreased at higher EG concentrations. This shows the ability of EG to solvate the crystal surfaces and explains the deterioration of the mechanical properties of nylons exposed to higher concentration of EG. The changes in the index of crystalline density also show that EG is more effective than water in its ability to change the average nature of the crystals at 120 °C; the difference is less significant at 140 °C. In other words, ethylene glycol is more effective than water in increasing the crystal size and perfection, especially at lower temperatures.

One obvious effect of EG in N6, which has two crystalline forms γ and α, is that the γ to α conversion at 120 °C is more extensive with EG than with water. The α crystalline form is thermodynamically favored and is obtained during slow crystallization, whereas the γ form is kinetically favored and is obtained during rapid crystallization. The conversion of one crystalline form to another usually requires melting, or the formation of an intermediate amorphous phase, and recrystallization. Because stress alone could transform γ to α,[32] it is possible that γ to α transformation could occur in the solid state within the lamellae without the "melting" of the γ crystals. Our observation of the more extensive diffusion of EG through the fold surface compared to water and the concomitant extensive transformation of γ to α leads us to speculate that such crystalline transformation are initiated at the fold surface.

The data in Figure 8 show that N66 crystals continue to resist the diffusion of EG at temperatures higher than N6. In other words, that EG diffuses more readily into

N6 than into N66. The changes which occur at ~120 °C in N6 occur at ~160 °C in N66. This difference in the temperature at which N6 and N66 undergo structural changes as seen in the SANS data are consistent with differences in the melting temperature (T_m). DSC scans show that the T_m of the two nylons in the presence of water or ethylene glycol is depressed. The T_m's are sensitive to the conditions used measurement, e.g., the amount of solvents and the heating rates. For instance, we occasionally observed a 144 °C melting endotherm in the presence of EG in both N6 and N66. But the most reproducible measurements show that T_m of N6 decreases from 224 to 200 °C in water and to 189 °C in EG, and the T_m of N66 decreases from 264 to 245 °C in water and to 207 °C in EG. These results show that the differences in the T_m between N6 and N66 appear to be conserved in the presence of water or EG, and therefore the mechanisms which depress the T_m can also account for the temperature at which water or EG is able to diffuse through the amorphous domains in the nylons. It is possible that the mobility amorphous chain segments at the surface of the lamellae which affect the melting point by changing the surface energy also affect the diffusion process. The structures at the fold surface in each of the two polymers are expected to be different. The crystalline stems in N6, unlike those in N66, have to form hydrogen bonds only between antiparallel chains. However, no such constraints exist in the amorphous regions. The differences in the amorphous domains in the interlamellar regions in the two nylons can therefore be attributed to the differences in the structure at the crystal surface. We speculate that the changes we observe in the interlamellar regions where water or EG interacts with the fold surface contribute to the observed deterioration in the properties of nylons exposed to EG at elevated temperatures.

Conclusions

(1) A wide range of SANS data can be fitted with a simple model in which the central diffuse scattering is attributed to independently scattering deuterium-rich domains outside the lamellar stacks and lamellar scattering is due to the deuterium contrast within the lamellar stack.

(2) About 2/3 of the amorphous chains are outside the lamellar stacks. The crystallinity within the lamellar stacks is about 80% and is almost independent of the overall crystallinity of the sample.

(3) The thickness of the interlamellar amorphous layers which take up water can be determined by analyzing the diffuse background under the lamellar peak. The apparent shifts in the lamellar spacings is attributed to the changes in the width or the shape of the scattering length distribution function.

(4) Density differences due to ND-c and ND-a alone give rise to a weak lamellar peak, and the contrast due to ND-c and NH-a is sufficient to give rise to an intense lamellar peak.

(5) Structural changes in nylons are more severe with EG than with water. This is consistent with the larger depression in the melting temperature with EG than with water (40 and 60 °C in EG for N6 and N66 compared to 20 °C in water for both N6 and N66).

(6) EG diffuses into the crystal surface (possibly the fold surface) at elevated temperatures, 120 °C in N6 and above 140 °C in N66. This difference could be due to the differences in the structure of the folds in the two nylons. EG facilitates the transformation of γ to α by increasing the mobility at the fold surface.

(7) Changes within the lamellae at elevated temperatures also bring about changes in the interlamellar regions. A transition observed at 125 °C in hydrated nylons is attributed to the crystalline relaxation that also bring about the Brill transition at 160°C in dry nylons.

Acknowledgment. We thank. S. Krueger, P. Thiyagarajan, and D. Wozniak for their generous help in obtaining the SANS data, J. Belles for the DSC scans, C. Bednarczyk for some of the experimental work, and Dr. W. Wu and Prof. B. Crist for helpful discussions. The SANS work at NIST is funded by the National Science Foundation under the Agreement No. DMR-9122444, and that at the IPNS (Argonne National Laboratory) by the U. S. Department of Energy, BES-Materials Science under Contract W-31−109-ENG-38.

References and Notes

(1) Murthy, N. S.; Correale S. T.; Minor, H. *Macromolecules* **1991**, *24*, 1185.
(2) Murthy, N. S.; Minor, H.; Bednarczyk C.; Krimm, S. *Macromolecules* **1993**, *26*, 1712.
(3) Campbell, G. A. *J. Polym. Sci. Poly. Lett*. **1969**, *7*, 629.
(4) Hinrichsen, G. *Colloid Polym. Sci.* **1978**, *256*, 9.
(5) Fischer, E. W.; Herchenröder, P.; Manley, R. St.; Stamm, M. *Macromolecules* **1978**, *11*, 213.
(6) Murthy, N. S.; Stamm, M.; Sibilia, J. P.; Krimm, S. *Macromolecules* **1989** *22*, 1261.
(7) Miura, H.; Hirschinger, J.; English, A. D. *Macromolecules* **1990**, *23*, 2169.
(8) Plestil, J.; Baldrain, J.; Ostanevich, Y. M.; Bezzabotnov, V. Y. *J. Polym. Sci., Polym. Phys.* **1991**, *29*, 509.
(9) Vergelati, C.; Imberty, A.; Perez, S. *Macromolecules* **1993**, *26*, 4420.
(10) Murthy N. S.; Orts, W. J. *J. Polym. Sci., Polym. Phys.* **1994**, *32*, 2695.
(11) Jen, X.; Ellis, T. S.; Karasz, F. E. *J. Polym. Sci., Polym. Phys.* **1984**, *22*, 1701.
(12) Papir, Y. S.; Kapur, S.; Rogers, C. E.; Baer, E. *J. Polym. Sci., Part A-2* 1972, *10*, 1305.
(13) Hutchison, J. L.; Murthy, N. S.; Samulski, E. T. *Macromolecules* **1996**, *17*, 5551.
(14) Sauer, B. B; Hsiao, B. S. *Polymer* **1995**, *36*, 2553.
(15) Murthy N. S.; Minor, H. *Polymer* **1990**, *31*, 996.
(16) Strobl, G. R.; Schneider, M. J. *J. Polym. Sci., Polym. Phys.* **1980**, *18* 1343.
(17) Wenig, W.; Bramer, R. *Colloid Polym. Sci.* **1978**, *256*, 125.
(18) Cameraon, R. E.; Donald, A. M. *Polymer* **1992**, *33*, 2628.
(19) Jenkins, P. J.; Donald, A. M. *Polymer* **1996**, *37*, 5559.
(20) Bracewell, R. *The Fourier Transform and Its Applications* McGraw Hill: New York, 1965.
(21) Vonk, C. G. *J. Appl. Crystallogr.* **1973**, *6*, 81.
(22) Vonk, C. G. In *Small-angle X-ray Scattering*; Glatter, O. Kratky, O., Ed.; Academic Press: New York 1982; p 447.
(23) Murthy N. S.; Orts, W. J. *Proc. ACS Div. Polym. Mater.: Sci. Eng.* **1994**, *71*, (Fall), 293.
(24) Statton, W. O. *J. Polym. Sci.* **1962**, *58*, 205.
(25) Heyn, A. N. J. *Text. Res. J.* **1963**, *23*, 782.
(26) Murthy, N. S.; Reimschuessel, A. C.; Kramer,V. *J. Appl. Polym. Sci.* **1990**, *40*,249.
(27) Santa Cruz, C.; Stribeck, N.; Zachman H. G.; Balta Calleja, F. J. *Macromolecules* **1991**, *24*, 5980.
(28) Murthy, N. S. *J. Polym. Sci., Polym. Phys.* **1986**, *24*, 549.
(29) Starkweather, H. W. Transitions and Relaxations In *Nylon Plastics Handbook* Kohan, M. I., Ed., Hanser, Munich, Germany, 1995; p 140.
(30) Murthy, N. S.; Curran, S. A. Aharoni S. M.; Minor, H. *Macromolecules* **1991**, **24**, 3215.
(31) Murthy, N. S.; Minor H.; Latif, R. A. *Macromol. Sci.—Phys.* **1987**, *B26*, 427.
(32) Murthy, N. S. *Polym. Commun.* **1991**, *32*, 301.

MA9707603